Super-resolution enhancement of Sentinel-2 image for retrieving LAI and chlorophyll content of summer corn

Mingzheng Zhang [1, 2], Wei Su [1, 2*], Yuting Fu [3], Dehai Zhu [1, 2], Jing-Hao Xue [4], Jianxi Huang [1, 2], Wei Wang [1, 2], Jiayu Wu [1, 2], Chan Yao [1, 2]

[1] College of Land Science and Technology, China Agricultural University, Beijing 100083, China
[2] Key Laboratory of Remote Sensing for Agri-Hazards, Ministry of Agriculture and Rural Affairs, Beijing 100083, China;
[3] Department of Mathematical Sciences, Tsinghua University, Beijing 100084, China
[4] Department of Statistical Science, University College London, London, WC1E 6BT, UK
* Correspondence: suwei@cau.edu.cn; Tel.: +86 010-6273-7855

Received: date; Accepted: date; Published: date

Abstract: Sentinel-2 satellite is a new generation of multi-spectral remote sensing technique with high spatial, temporal and spectral resolution. Especially, Sentinel-2 incorporates three red-edge bands with central wavelength at 705, 740 and 783 nm, which are very sensitive to vegetation changing, heath and variations. Unfortunately, their spatial resolution is only 20 m, which is lower comparably. This spatial resolution brings difficulties for mining the potential of Sentinel-2 image in vegetation monitoring. Therefore, we focus on enhancing the spatial resolution of Sentinel-2 red edge band images to 10m using the SupReME algorithm. Furthermore, the summer corn canopy leaf area index (LAI), leaves chlorophyll content (LCC) and canopy chlorophyll content (CCC) were retrieved by the linear and physical models for the corn growth monitoring purpose. The results showed that the spatial resolution of Sentinel-2 images had been enhanced to 10m from original 20m, and the estimation accuracy (EA) was over 97% for pixels planted by summer corn. Moreover, the accuracy of summer corn canopy LAI, LCC and CCC was improved respectively using enhanced Sentinel-2 images by SupReME method. During these three parameters retrieval, the red-edge bands or SWIR bands were introduced into optimal cost function and vegetation index which the accuracy of these models was high. The SupReME algorithm provides a valuable way for Sentinel-2 images enhancement, which is of great potential to mining Sentinel-2 images and multitude its application.

Keywords: Sentinel-2 image; SupReME algorithm; LAI; chlorophyll content; radiative transfer model

1. Introduction

Accurate estimation of vegetation biophysical variables with high spatial and temporal resolution plays an important role in global climate change monitoring, comprehensive monitoring of land use/cover change, estimating the total amount of ecological resources etc.(Guan et al., 2016, 2017; Houborg et al., 2007; Boegh et al., 2002; Huang et al., 2015). Simultaneously, parameters obtained from remote sensing observation data are very important inputs for energy and material exchange models between vegetation and the external environment (Baret et al., 2006,2007; Darvishzadeh et al., 2008), including leaf area index (LAI), leaves chlorophyll content (LCC) and canopy chlorophyll content (CCC) and so on.

Optical satellite imagery is one of the important data sources for vegetation biophysical variables estimation. With the development of aerospace technology, there are more and more available satellite images with increased temporal resolution, spatial resolution and spectral resolution (Gascon et al., 2009). Sentinel-2 is a new generation of multi-spectral imagery with 13 spectral bands, including three red-edge bands which are sensitive to the chlorophyll content of

vegetation (Sibanda et al., 2015; Atzberger et al., 2012; Pu et al., 2003). It is an ideal data source for vegetation growth monitoring and is used for terrestrial observations of global high resolution and high revisiting capabilities, biophysical change mapping, monitoring of coastal and inland waters, and risk and disaster mapping to support the continuity of SPOT-5 and Landsat satellite data (Wang et al., 2017; Clevers et al., 2013). The difference in spatial resolution constrained by technical conditions and cost inputs also appears in other satellite images, for instance, MODIS, Landsat and Worldview-3. The Sentinel-2 image is in the same way, with 20m spatial resolution within three red edge bands and not balance to the 10m spatial resolution of visible bands and Near Infrared (NIR) band. It is a balancing strategy of high Signal Noise Ratio and spatial resolution for each channel. However, the availability of 10m images provides an opportunity to improve the resolution of other 20m images, leading to an effective means to maximize output without increasing input costs.

Image super-resolution enhancement is a prospective approach to using signal processing techniques to obtain a high spatial resolution image (or sequence) from observed multiple low-resolution images (Park et al., 2003). At present, many researchers have focused on super-resolution enhancement and developed a variety of feasible algorithms. The pan-sharpening approach refers to the fusion of panchromatic and multispectral images which could improve the spatial resolution of the multispectral images and reduce spectral distortion synchronously (Thomas et al., 2008). Vivone et al. (2015) used five data sets acquired by different satellites to evaluate the performance of various pansharpening algorithms, including component substitution and multiresolution analysis (MRA), and their results indicate that the overall performance of MRA was generally better than those of others. Wang et al. (2015, 2016) proposed an algorithm called area-to-point regression kriging (ATPRK) that used MODIS bands 1 and 2 with 250m spatial resolution to downscale the 500m spatial resolution of MODIS bands 3-7 to produce a set of 250m spatial resolution MODIS images. The result of ATPRK was of high quality and showed great potential in MODIS images applications. Pardo-Iguzquiza et al. (2011) extended the method of spatially adaptive cokriging filter for fusing the high spatial resolution panchromatic band 8 image (i.e., 15m) and the low spatial resolution multispectral band 2 (i.e., 30m) of Landsat ETM+ to generate image with 15m resolution. In these studies, the high-resolution images used are the panchromatic bands, the average values of several high-resolution images or one high-resolution image which has similar central wavelength with low-resolution image. However, they cannot make full use of the advantages of multispectral high-resolution images. Lanaras et al. (2017) proposed a high-quality solution algorithm called SupReMe that took only one step to get the highest available resolution image in all lower-resolution channels. The SupReMe algorithm is based on variable segmentation to obtain an equivalent constrained optimization formula, and then it is solved by the augmented Lagrangian method (Afonso et al., 2010). Furthermore, this approach has been tested on simulated and real Sentinel-2 images, and the best results have been obtained compared with other methods.

The multispectral images with high spatial resolution obtained by downscaling provides reliable data support for accurate inversion of vegetation growth parameters (Huang et al., 2015, 2016). It is also an important and promising product widely used in the remote sensing field. Few investigators have focused on the capability of super-resolution fusion image (i.e. 10m for all bands) on quantitative estimation and evaluation of vegetation growth for Sentinel-2 satellite. At present, there are two kinds of inversion programme, statistical regression models and physical models, and more band choices make these two methods have broad application prospects. Firstly, prior investigations (Turner et al., 1999; Carlson & Ripley, 1997; Chen & Cihlar, 1996) have demonstrated that there is a significant linear relationship between vegetation growth parameters and vegetation index. Although it is simple and efficient, it depends on the measured data and vegetation types on the ground and has poor universality. Besides that, physical models are an important way to understand the relationship between vegetation spectrum and vegetation growth (Darvishzadeh et al., 2008; Houborg et al., 2007, 2008; Gastelluetchegorry et al., 1996; Kuusk, 1995). The physical models could simulate a complete spectral curve (400-2500nm) by inputting vegetation parameters and we can use the limited satellite observation channels to approximate this curve as far as

possible, then retrieve the corresponding vegetation parameters (Combal et al., 2003). Compared with the earlier satellites, which only have four effective bands of blue, green, red and NIR, the latest satellite Sentinel-2 with 13 bands has more obvious advantages in vegetation inversion.

Therefore, this study is focusing on enhancing Sentinel-2 multi-spectral images with different spatial resolutions to generate high spatial resolution multi-spectral images using the SupReMe algorithm, aiming at improving the retrieving accuracy of summer corn canopy LAI, LCC and CCC. For this purpose, we have formulated following study contents:

(i) Analyzing the performance, stability and effect of the SupReMe algorithm in super-resolution enhancement ;

(ii) Retrieving summer corn canopy LAI, LCC and CCC using empirical model and physical model, and discussing the ability variance in retrieving parameters between enhanced images and original Sentinel-2 images;

(iii) Exploring the effects of band combinations on retrieval of LAI, LCC and CCC by ordering combination;

(iv) To evaluate the retrieval accuracy of LAI, LCC and CCC, for mining the potential of Sentinel-2 images with SupReMe algorithm in agriculture.

2. Materials and Methods

2.1. Study area

The study area is located in Yongqing County, Anci District and Guangyang District of Langfang City, Hebei Province (39°05′N~39°40′N,116°20′E~116°55′E), which is located the middle-east of North China Plain (as shown in Fig.1). It is in the mid-latitude zone with warm temperate continental monsoon climate. The average annual temperature is about 10~12°C and the average annual precipitation is 554.9 mm. The dominated terrain is plains with an average elevation of about 13m. The predominant tillage pattern is an intensive dual-cropping system between winter wheat, spring corn, summer corn, soybean, potatoes, and vegetables and so on. In general, the growing season of summer corn in study area is from the end of June to the early October.

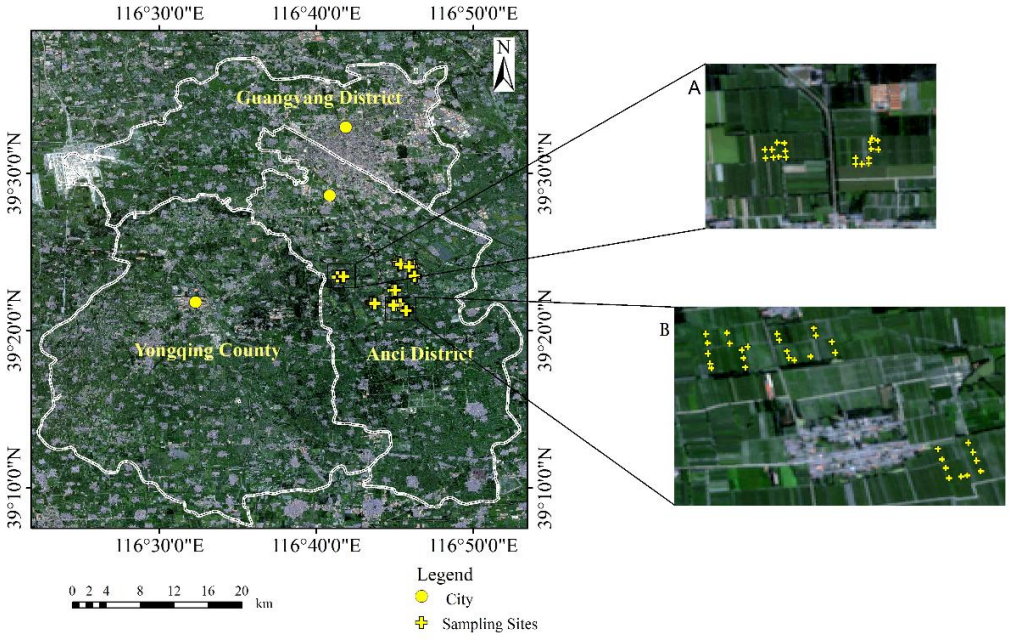

Fig. 1. The research area (R/G/B=Band4/Band3/Band2)

2.2. Sentinel-2A image and preprocessing

The Sentinel-2A Level-1C images with 10m and 20m spatial resolution (Fig. 1) were used in this study, and the spatial resolution and spectral range were listed in Table 1. The cloudless Level-1C products were acquired on 21 August 2018 at 11:05 UTC with UTM/WGS84 projection were used for

image enhancement. Sen2cor (Muller-wilm et al., 2013) model (version sen2cor-2.5.5) was used to do atmospheric correction for studied Sentinel-2A image, which converted the top of atmosphere reflectance to the bottom of atmosphere reflectance. In order to get the same amount of pixels for each image band the nearest neighbor method was used to resample the 20m images to 10m (specific bands were shown in Table 1). This resampling operation guarantee the consistency of pixel size and reflectance before and after image enhancement. In the next step, the supervised classifier was used to extract the corn planted area for corn canopy LAI and chlorophyll content retrieval.

Table 1. List of Sentinel-2 image band parameters

Spatial resolution (m)	Band	Central wavelength (nm)	Band width (nm)
10	Band2-Blue	490	65
	Band3-Green	560	35
	Band4-Red	665	30
	Band8-NIR	842	115
20	Band5-Red edge	705	15
	Band6-Red edge	740	15
	Band7-Edge of the NIR plateau	783	20
	Band8a-Narrow NIR	865	20
	Band11-SWIR	1610	90
	Band12-SWIR	2190	180

2.3. Field campaign

The in-situ measurements of corn canopy parameters were done in the study area from 22 to 26 August, 2018. The phenological stage of corn in the study area ranged from the heading stage to the milky stage because of the difference of planting time between different fields. Corresponding to Sentinel-2 image resolution (10m), 113 quadrats with the size of 5m×5m were selected to do in-situ measurements (Fig. 1). The measured parameters included LAI, average leaf inclination angle (ALIA), LCC. The location of all the quadrats was provided using a Huace i80 real-time kinematic (RTK) GPS receiver (Huace Ltd., Shanghai, China). The sampling pattern in each quadrat and the sketch of leaf chlorophyll content measurements were shown in Fig. 2. In one quadrat, LAI and LCC were measured at location A and B (the location of A and B is random, but the distance between the two points is 2-3 meters); C represents the center of the quadrat and we only measured the coordinates at C by RTK to indicate the position of the quadrat.

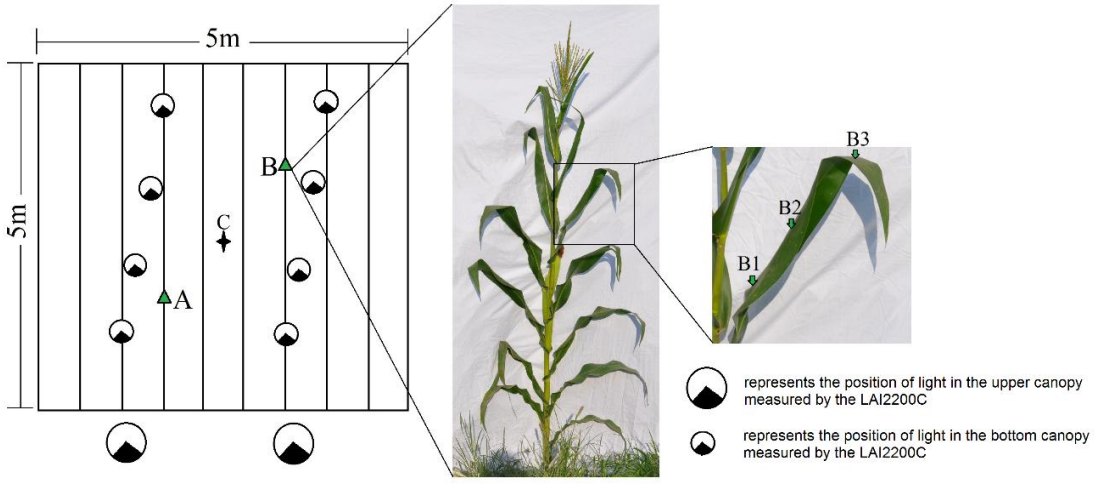

Fig. 2. Sampling pattern in each quadrat and the sketch of leaf chlorophyll content measurements: A and B represent two corn plants with uniform growth in the sample; C represents the center of the sample and records coordinates with RTK; B1~B3 represent the location of LCC measured by SPAD-502Plus in one leaf.

LAI was measured in the field using the Plant Canopy Analyzer LAI-2000C (LICOR Inc., Lincoln, NE, USA). The method was the indirect optical method that the LAI and ALIA were calculated by Beer-Lambert law from the transmittance of the canopy (Welles and Norman, 1991).

We measured LAI at each quadrat on the position A and B, and the average value was used as the inputs of PROSAIL model. Meanwhile, the SPAD-502Plus Leaf Chlorophyll Meter (MINOLTA, Inc.) was used to measure the chlorophyll content of corn leaves nondestructively (Campbell et al., 1990) on the position A and B. When measuring chlorophyll content, two or three corn plants were selected to measure chlorophyll content per leaf in each sample plot; six leaves on the top of plant were selected, and three chlorophyll values were measured from the base to the tip of each leaf. The SPAD readings (unitless) are highly correlated with leaf chlorophyll content (LCC, μg/cm²) in leaves which could be converted by means of an empirical calibration function (Darvishzadeh et al., 2011; Markwell et al., 1995):

$$LCC = 10^{SPAD^{0.264}-4} * M \quad (1)$$

where SPAD was the reading value of the SPAD-502Plus; and M means molar mass of chlorophyll, and the average value 907g/mol was used in this study. The average value of all in-situ measured leaf chlorophyll content values within one sampling plot was used as the chlorophyll content of studied sampling plot. Furthermore, the canopy chlorophyll content (CCC) was calculted by the product of leaf chlorophyll content and LAI:

$$CCC = LAI * LCC \quad (2)$$

The measured LAI, ALIA and LCC for 113 quadrats were analyzed in this sutdy. It was found that these growth parameters of summer corn in study area were approximately Gaussian distributed (as shown in Fig.3), which also provided a priori knowledge for parameter input and sensitivity analysis of the later physical model.

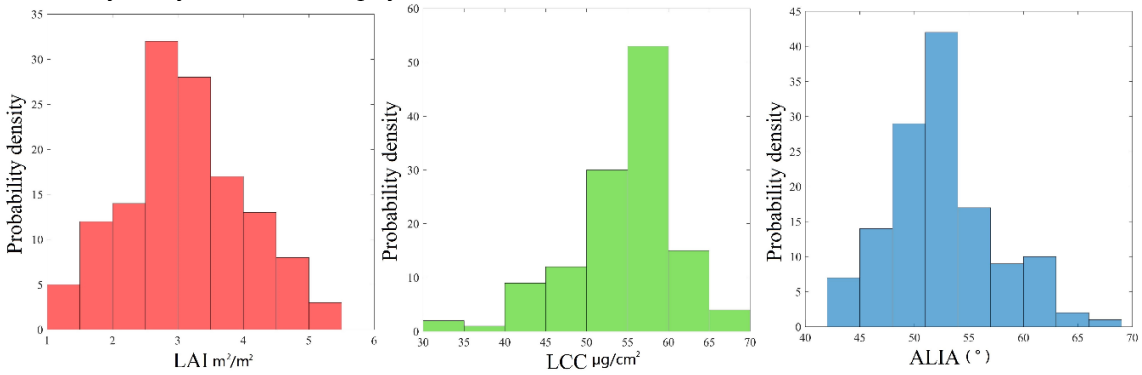

Fig. 3. The probability density distribution of the measured LAI, LCC and ALIA

2.4. Image enhancement by SupReME algorithm

The super-resolution enhancement method used in this study is SupReME (Super-Resolution for Multispectral Multiresolution Estimation) algorithm (Lanaras et al. 2017). The advantage of this algorithm is that it has high automation and fast computational efficiency which could process all bands of Sentinel-2 image once to generate data sets with the high spatial resolution of 10m. This method relies on the observation model of the imaging (blurring and down sampling) process that generates the low-resolution images, i.e. the output image $X = [x_1^T; \ldots; x_L^T] \in R^{L \times n}$ (a fixed image area contains n high-resolution pixels) is blurred and downsampled as the observed image $y = (y_1, \ldots, y_L)$ with L spectral bands. Vectorise X as $x = (x_1, \ldots, x_L)^T \in R^{Ln}$, x and y are related through

$$y = MBx \quad (3)$$

where the blur matrix B is a block-circulant-circulant-block matrix where each block represents a 2D cyclic convolution, and M is block-diagonal and the blocks represent the sampling of x to represent y and $R^{L \times n}$ represents a set of vectors consisting of all $L \times n$ dimensional vectors.

In the continuous spectral curve, the two adjacent bands have strong correlation. Therefore, dimensionality reduction of high-dimensional hyperspectral images can be carried out without losing information. We assume that the columns of X lies in a subspace spanned by the columns of U, i.e. $X = UZ$, vectorise form: $x = (U \otimes I)z$, where I is an identity matrix with suitable dimensions.

Estimation of the subspace U:

(i) Upsample all the bands of y to the same high resolution, using bicubic interpolation.
(ii) Blur each band, such that the blur of all the bands is equivalent to the strongest blur.
(iii) Perform singular value decomposition on the blurred data. Retain the singular vectors of p largest singular values as the columns of U.

Then image fusion can be formulated as a convex optimization problem:

$$\min_{z} ||MB(U \otimes I)z - y||^2 + \lambda\phi_{w,q}(D_h z, D_v z) \quad (4)$$

where $\phi_{w,q}$ is a quadratic regularisation term, based on weights w, q and λ is the regularization strength; and $D_h, D_v \in R^{Ln \times Ln}$ are two block-diagonal linear operators (each with identical blocks) that approximate horizontal and vertical derivatives of the images in z. For simplicity, we treat these matrices with periodic boundary conditions as cyclic convolutions.

The above minimization problem (Eq 4) is equivalent to

$$\min_{z,v_1,v_2,v_3} ||MBv_1 - y||^2 + \lambda\phi_{w,q}(v_2, v_3) \quad (5)$$
$$\text{s.t. } v_1 = (U \otimes I)z$$
$$v_2 = D_h z$$
$$v_3 = D_v z$$

The Augmented Lagrangian of Eq 4 is

$$L(z, v_1, v_2, v_3, d_1, d_2, d_3) \quad (6)$$
$$= ||MBv_1 - y||^2 + \lambda\phi_{w,q}(v_2, v_3) + \frac{\mu}{2}||(U \otimes I)z - v_1 - d_1|| + \frac{\mu}{2}||D_h z - v_2 - d_2|| + \frac{\mu}{2}||D_v z - v_3 - d_3||$$

where d_1, d_2, d_3 are scaled Lagrange multipliers and weight $\mu > 0$

Iteratively optimize three parameter blocks:$z, (v_1, v_2, v_3)$ and (d_1, d_2, d_3) we can obtain the optimal z, and then get x by $x = (U \otimes I)z$. For more information, you can see in Lanaras et al. (2017) and the code of the SupReME algorithm can be downloaded publicly on the GitHub (https://github.com/lanha/SupReME).

To quantify the performance of the SupReME algorithm, the reflectance of enhanced images and original images were calculated for each band and the following statistics were calculated (Eqs.7-9): coefficient of determination (R^2), the root mean squared error (RMSE) and estimation accuracy (EA). In detail, the calculation formulas are as follows:

$$R^2 = \frac{\sum_{i=1}^{n}(\hat{y}_i - \bar{y})^2}{\sum_{i=1}^{n}(y_i - \bar{y})^2} \quad (7)$$

$$RMSE = \sqrt{\frac{\sum_{i=1}^{n}(\hat{y}_i - y_i)^2}{n}} \quad (8)$$

$$EA = \left(1 - \frac{RMSE}{\bar{y}}\right) \times 100\% \quad (9)$$

where n is the number of pixels, $\hat{y}_i$ is the estimated value of pixel in the fusion image, $\bar{y}$ is the average value of pixel in the original image, and y_i is the value of pixel in the original image.

2.5. Corn canopy parameters estimation using vegetation index

Vegetation index (VI) is an empirical measurement of vegetation activity, which is calculated by combining two or more spectral observation channels (Meroni et al., 2004). Vegetation index, as a means of characterizing surface vegetation coverage and growth in the field of remote sensing, has higher sensitivity than single-band detection vegetation growth and is widely used to invert vegetation biophysical parameters, such as LAI and LCC. There are two forms of vegetation index in common use (Darvishzadeh et al., 2008), ratio index (RI, Eq.7) and normalized difference index (NDI, Eq.8):

$$\text{RI} = \frac{R_a}{R_b} \quad (10)$$

$$\text{NDI} = \frac{R_a - R_b}{R_a + R_b} \quad (11)$$

where R_a and R_b represent the two spectral channels of the Sentinel-2 image, respectively. There are 10 bands with the enhanced 10m Sentinel-2 image which makes it possible to retrieve an optimal

band combination. We traversed all two bands combination to build a linear model, and then analyzed the result of R^2 and RMSE to find the optimal model. Finally, they were validated by the measured data. (Zhao et al., 2007).

In view of the limitation of spatial and spectral resolution of early satellite, the vegetation index is usually composed of red band and NIR band. Undeniably, ground experiments proved that the red-edge band (670-760nm) is an important indicator band for describing the state of plant pigments and health (Vina et al., 2011; Brantley et al., 2011). Therefore, the red-edge band is an ideal channel for remote sensing to investigate vegetation status and estimate vegetation parameters (Delegido et al., 2011). Thus, we also tested three other commonly used VIs, including Modified Chlorophyll Absorption Ratio Index (MCARI) (Daughtry et al., 2000), MERIS Terrestrial Chlorophyll Index (MTCI) (Dash & Curran, 2007) and the Angular Insensitivity Vegetation Index (AIVI) (Li et al, 2016). The formulas and references are as follows:

$$MCARI = [(Band6 - Band5) - 0.2 * (Band6 - Band3)] * \frac{Band6}{Band5} \quad (12)$$

$$MTCI = \frac{Band6 - Band5}{Band5 - Band4} \quad (13)$$

$$AIVI = \frac{Band2 * (Band5 + Band6) - Band3 * (Band5 - Band6)}{Band5 * (Band3 + Band2)} \quad (14)$$

The pixel size of enhanced image is 10m×10m, and the reflectance of a single pixel is a mixed spectrum of the whole vegetation canopy. We inverted LAI and CCC directly from canopy spectra, and then calculated LCC by the ratio of CCC to LAI.

In this study, we separated the measured data of 113 quadrats by the stratified sampling. That is all sample points are divided into five layers according to the size of LAI value, and sample points of each layer are randomly divided into two parts. Finally, 63 of them were used for calibration of linear model and 50 of them were used for accuracy validation of LAI, LCC and CCC retrieval.

2.6. Corn canopy parameters retrieval using PROSAIL model

Compared with vegetation indexes, the physical radiative transfer model is based on rigorous mathematics, physics and biology process, which can explain clearly the interaction mechanism between solar radiation and the canopy, and has strong applicability. Furthermore, the physical model can determine the bidirectional reflectance distribution function of the canopy to quantitatively describe the distribution of light in the canopy (Roy et al., 2017; Bousquet et al., 2005). Therefore, we retrieve LAI and chlorophyll content using PROSAIL-D (Berger et al., 2018) radiative transfer model in this study. The PROSAIL-D model is the coupling of the leaf-scaled PROSPECT-D (Féret et al., 2017) model and the canopy-scaled Scattering by the Arbitrarily Inclined Leaves (SAIL) model (Jay et al., 2017; Jacquemoud et al., 2009) (see Fig. 4). The PROSECT-D model is used for dense and non-dense leaf vegetation that describes the transmission of light on the surface and inside of leaves, which increases the anthocyanin content (Canth) of leaves compared with PROSECT-5 (Allen et al., 1969; Féret et al., 2009). The SAIL model is one of the commonly used models for descripting vegetation canopy and it assumes that vegetation canopy is a mixture of horizontal, homogeneous and infinitely extended isotropic leaves with random azimuth distribution.

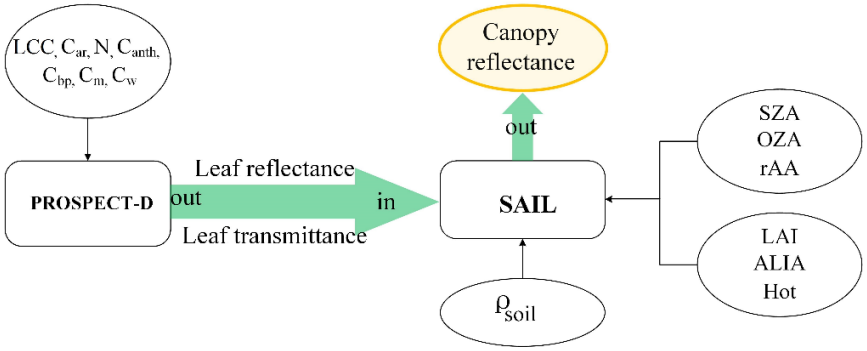

Fig. 4. Simulation the canopy reflectance by PROSAIL-D model

The ill-posed problem always exists in vegetation canopy parameters retrieval, such as retrieving LAI, canopy chlorophyll content etc. In other words, the vegetation canopy parameters cannot be directly obtained by inputting canopy reflectance with less prior information. Improved Look-up table (LUT) (Darvishzadeh et al., 2012) and cost function ($J(x)$) (Casa & Jones, 2004; Nilson & Kuusk, 1989) are used to alleviate this problem in this study.

A summary of the range and distribution of PROSAIL model inputs used in this study is shown in Table 2, which are used to determine the dimension of LUT. The distribution and range of parameter LCC, LAI and ALIA are obtained from the measured data in field campaign. These inputs including Car, Canth, LCC, Cm, Cw, N, ϱsoil and Hot, are determined by referencing the prior knowledge and data base of Leaf Optical Properties Experiment 93 (Andreoli & Hosgood, 1994). Parametric SZA and OZA are recorded in the header file of the Sentinel-2 image, and rAA is determined by subtracting the azimuth angles of the sun and satellite. The observation zenith angle and observation azimuth angle of Sentinel-2 are different in each band, but generally less than 5°. In this study, we used the average value of the observation zenith angle and observation azimuth angle of satellite to retrieve vegetation parameters.

Table 2. The ranging and distribution of PROSAIL-D model inputs for producing the LUT

Parameters	Units	Max	Min	Mean	Std	Distribution
LCC	μg/cm²	70	30	55	15	Gaussian
Car	μg/cm²	10	2	6	2	Gaussian
Canth	μg/cm²	10	2	6	2	Gaussian
Cbp	μg/cm²	——	——	0.2	——	default
Cm	cm	0.006	0.003	0.004	0.001	Gaussian
Cw	g/cm²	0.03	0.01	0.0131	0.005	Gaussian
N	——	——	——	1.518	——	default
ϱsoil	——	——	——	0.8	——	default
LAI	m²/ m²	6	1	3.5	2	Gaussian
ALIA	°	65	45	50	10	Gaussian
Hot	——	——	——	0.1	——	default
SZA	°	——	——	30.22	——	default
OZA	°	——	——	7.73	——	default
rAA	°	——	——	135.21	——	default

When the LUT is generated, the minimum cost function ($J(x)$) can be used to retrieve the simulated reflectance closest to the observed reflectance, and then extract the corresponding vegetation canopy parameters. The cost function is

$$J(x) = \sum_{i=1}^{n} \lambda_i \left(R_i^{LUT} - R_i^{observe}\right)^2 + \sum_{j=1}^{m} \left[\left(x_j - x_{j,b}\right)^2 \gamma_j\right]^2 \quad (15)$$

where n is the number of bands in the cost function, λ_i is the weight of ith band (for LAI, $\lambda_i = 1$, for LCC, $\lambda_i = 1/R_i^{observe}$), R_i^{LUT} the simulated canopy reflectance obtained from the PROSAIL-D model, $R_i^{observe}$ is the canopy reflectance observed by Sentinel-2 images, m is the number of penalty function parameters, x_j is the input of the parameter j of the model in the LUT, $x_{j,b}$ is the limit of parameter j(if $x_j < x_{j,min}$ or $x_j > x_{j,max}$, then γ_j is a maximum value(such as $\gamma_j = 100$)else, $\gamma_j = 0$). In the retrieval of summer corn canopy LAI, LCC and CCC, the estimated results of them using empirical vegetation indexes are used as prior knowledge to obtain the $x_{j,b}$ of penalty function. Generally, we take the 10% fluctuation of the results from the optimal linear model as its limit.

Furthermore, the band combination used for cost function is an important factor affecting the retrieval accuracy. The number of combinations M can be expressed as:

$$M = \sum_{n=1}^{10} C_{10}^{n} \quad (16)$$

In our case, n=10 and the number of combinations M is 1023. We built all kinds of cost function combinations, and validate the retrieval accuracy using these all kinds of cost functions with in-situ measured LAI and LCC in field campaign. The R^2 and RMSE are used to validate and find the optimal retrieving result.

3. Results and analysis

3.1. Evaluation of consistency between enhanced and original image reflectance

In order to evaluate the enhanced reflectance results from the developed SupReME algorithm, we validated the enhanced image qualitatively and quantitatively. Fig. 5 shows a detailed spatial comparison between original and enhanced Sentinel-2 reflectance images. We can find that the spatial details of the enhanced image (Fig. 5c and e) are in good agreement with that of the original 10m image (Fig. 5a). Compared with the original 20m images (Fig. 5b and d), there are clearer land objects boundaries, more detailed and clearer textural features for enhanced image, with the consistent spectral variation between different land objects between the original 20m image and the enhanced 10m image. In detail, the circled area is cropland planted with vegetables and summer corn, within which there is a trench full of algae passes through. In the original 10m natural color image (Fig.5a), it is difficult to distinguish the type of land objects because the spectrum of ditches which was covered with a thick layer of algae is similar to that of vegetation on the ground. In the original 20m images (Fig.5b, d), the difference between the ditch and the cropland can be seen roughly and weakly. Moreover, the boundaries of these two kinds of land objects are indistinct because of the small area of the objects and the low spatial resolution of the images. Comparably speaking, the boundary between the ditch and the farmland in the super-resolution 10m images (Fig.5c, 5e) is clearer and more distinct. Moreover, we can identify clearly the spectral characteristics of the objects are water and cropland, and the ditch is distinct, too. Therefore, we can conclude that the addition of multiband (Band5~7, 8a, 11, 12) can identify more spectral features of land objects. In general, the spatial resolution of the enhanced image has improved from 20m to 10m, and the spectral characteristics have not changed greatly before and after the image enhancement.

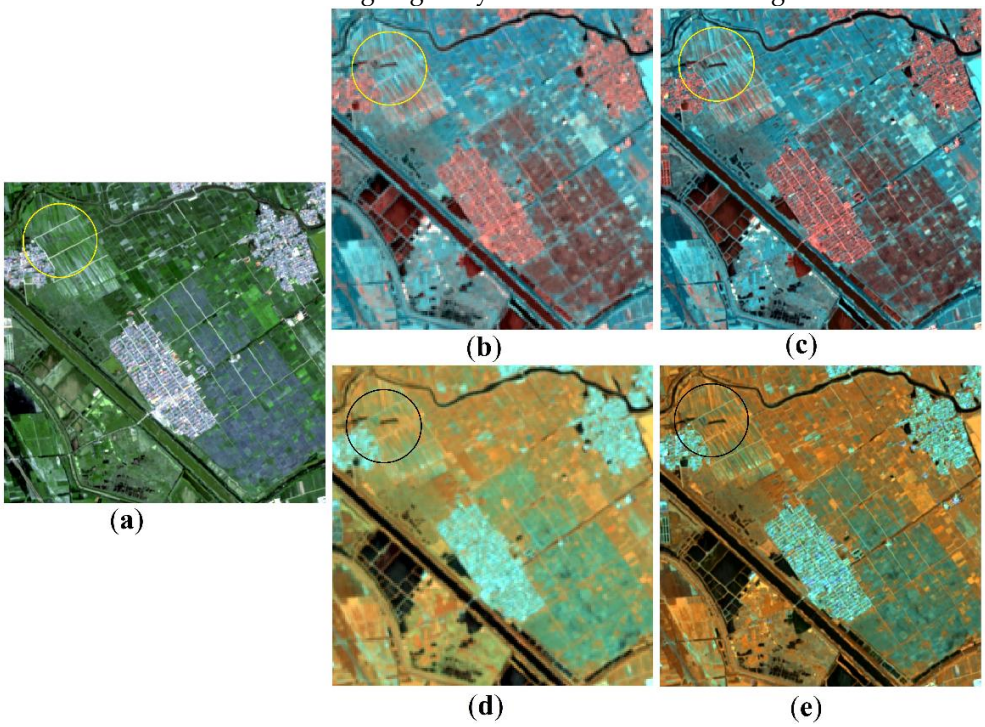

Fig. 5. Image fusion results using super-resolution algorithm: (a) Original 10m true color image, R/G/B=Band4/Band3/Band2; (b) Original 20m false color image, R/G/B=Band7/Band6/Band5; (c) enhanced 10m false color image, R/G/B=Band7/Band6/Band5; (d) Original 20m false color image, R/G/B=Band12/Band11/Band8a; (e) enhanced 10m false color image, R/G/B=Band12/Band11/Band8a.

Moreover, we evaluate the spectral consistency quantitatively between the enhanced 10m image using super-resolution method with the original 20m spatial resolution images (Band5~7, 8a, 11, 12), and focused on analyzing the spectral difference before and after super-resolution enhancement of Sentinel-2 image. Table 3 shows the spectral correlation for all bands of the original image and the enhanced image in the ranging area of 6000×6000 pixels.

From the analyzed spectral correlation in Table 3, we found that the reflectance of enhanced image was highly correlated with the original image. And correlation coefficient (R^2) between the original bands and enhanced bands are all greater than 0.87. The band with the highest correlation value is Band12 with R^2=0.99, and the band with the lowest correlation is Band11 with R^2 = 0.87. The EA of the whole image is higher than 79%, including corn planted area, roads, water etc. Fortunately, the EA in corn planted area is higher than 97% with the significant value at the 0.01 level. The correlation results in Table 3 revealed that the enhanced image using SupReME algorithm improves the spatial details of the image while maintaining the invariance of the spectrum. We found that the EA in the vegetation pixels of SupReME algorithm is higher than that of buildings, especially for Band11 and Band12.

Table 3. Correlation analysis result of image reflectance before and after enhancement

Band	Regression Equation	R^2	RMSE	EA%	EA%(R<0.6)
Band5	y=0.88x+0.0130	0.90**	0.0177	83.74	98.23
Band6	y=0.91x+0.0227	0.89**	0.0227	91.04	97.73
Band7	y=0.90x+0.0312	0.91**	0.0258	91.55	97.42
Band8a	y=0.88x+0.0397	0.91**	0.0273	91.54	97.25
Band11	y=0.82x+0.0375	0.87**	0.0268	86.55	97.31
Band12	y=0.88x+0.0164	0.99**	0.0277	79.29	97.22

Notes: ** Correlation is significant at the 0.01 level.

3.2. Estimating results of LAI and chlorophyll content using vegetation indexes

We developed RI and NDI by combing every two bands of the Sentinel-2 images and found the optimal vegetation index (Table 4) with the highest accuracy of corn canopy LAI and chlorophyll content estimation. Fig. 6 shows the comparations of the R^2 distributions retrieval results from different bands combination of enhanced image and original image. From Fig.6, it can be seen that the R^2 distributions of RI and NDI using enhanced image are similar, with the minor quantitative difference. The linear model (Fig. 6) has high accuracy when R_a = Band 3-Band 6 and R_b = Band 7-Band 11 for the original image and enhanced image. The difference between enhanced image and original image lies in that the enhanced image has higher R^2 than the original image. Moreover, we found that the result of RI and NDI has the highest R^2 in the LAI and CCC estimation when R_a= Band 8a and R_b = Band 3. For the original image, RI and NDI all have the best R^2 for the LAI and CCC estimation when R_a = Band 8 and R_b= Band 3,.

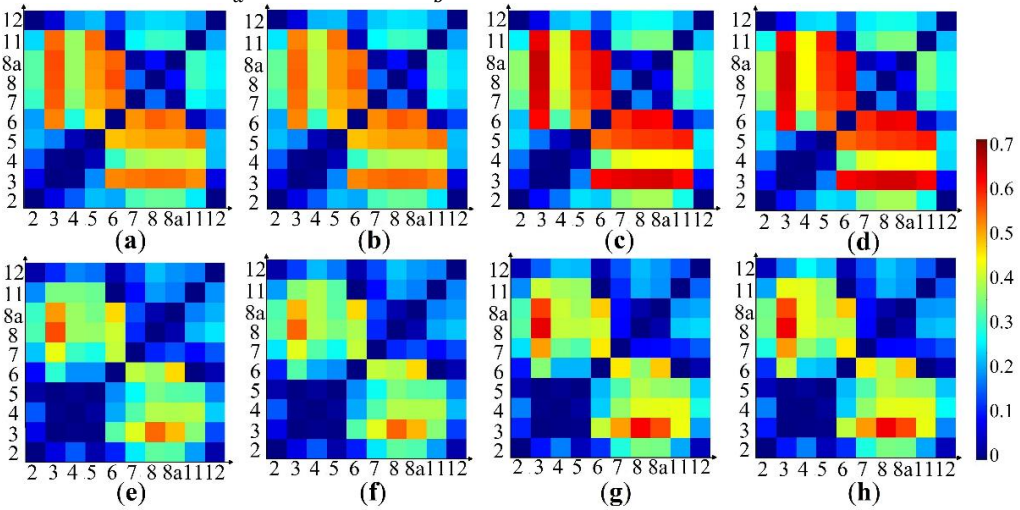

Fig. 6. The R^2 distribution results of LAI and CCC are inverted by different band combinations. The x and y axes are the respective bands of the image: (a, e) are R^2 of LAI estimated by RI of enhanced image and original image respectively; (b, f) are R^2 of LAI estimated by NDI of enhanced image and original image respectively; (c, g) are R^2 of CCC estimated by RI of enhanced image and original image respectively; (d, h) are R^2 of CCC estimated by NDI of enhanced image and original image respectively.

Furthermore, the MCARI, MTCI and AIVI (Table 4) were calculated for corn canopy LAI and CCC estimation. The optimal estimation results of LAI and CCC using RI and NDI calculated from enhanced image and original image showed that the narrow NIR band (Band 8a) had superiority and potential for estimating LAI and CCC, compared with NIR band (Band 8) which has similar central wavelength and the same spatial resolution. Comparably speaking, the narrow NIR band is more sensitive to corn growth difference and its changes.

The other three VIs used at least three bands in the process of construction, in which at least one band was red edge band with an original spatial resolution of 20 m. In conclusion, the estimated results using MCARI, MTCI and AIVI showed that the improvement of Sentinel-2 spatial resolution using the SupReME algorithm can improve the estimation accuracy of LAI and CCC.

Table 4. The estimation model of LAI and CCC using vegetation indexes

VI	Enhanced image		Original image	
	LAI	CCC	LAI	CCC
RI	$y=0.49e^{0.23x}$	$y=0.11e^{0.34x}$	**$y=0.58e^{0.21x}$**	$y=0.13e^{0.32x}$
	R^2=0.53** RMSE=0.52	R^2=0.60** RMSE=0.30	**R^2=0.51** RMSE=0.59**	R^2=0.52** RMSE=0.35
NDI	$y=0.01e^{7.48x}$	**$y=0.0002e^{11.64x}$**	$y=0.02e^{0.81x}$	**$y=0.0005e^{10.61x}$**
	R^2=0.55** RMSE=0.55	**R^2=0.63** RMSE=0.28**	R^2=0.50** RMSE=0.61	**R^2=0.56** RMSE=0.36**
MCARI	$y=0.74e^{0.21x}$	$y=0.19e^{0.31x}$	$y=0.77e^{0.20x}$	$y=0.18e^{0.31x}$
	R^2=0.49** RMSE=0.62	R^2=0.56** RMSE=0.37	R^2=0.40** RMSE=0.76	R^2=0.50** RMSE=0.48
MTCI	**$y=0.92e^{0.21x}$**	$y=0.28e^{0.30x}$	$y=0.88e^{0.20x}$	$y=0.25e^{0.30x}$
	R^2=0.57 RMSE=0.48**	R^2=0.57** RMSE=0.3	R^2=0.45** RMSE=0.66	R^2=0.52** RMSE=0.43
AIVI	$y=0.56e^{0.43x}$	$y=0.14e^{0.63x}$	$y=0.49e^{0.45x}$	$y=0.10e^{0.68x}$
	R^2=0.52** RMSE=0.50	R2=0.57** RMSE=0.29	R^2=0.49** RMSE=0.60	R^2=0.54** RMSE=0.36

Notes: ** Correlation is significant at the 0.01 level with n=63, x denotes the VIs and y denotes LAI or CCC.

Table 4 is the estimation accuracy of LAI and CCC using the optimal vegetation indexes, which are assessed using 50 in-situ measured samples in filed campaign. And the LCC was calculated by the ratio of the estimated CCC and LAI. For the reason that the value ranges of the three estimated parameters (i. e. LAI, CCC and LCC) are different, the normalized root mean square error (nRMSE) is chosen for the accuracy comparison. The calculating formulas is as followed:

$$nRMSE = \frac{RMSE}{y_{max} - y_{min}} \quad (17)$$

where y_{max} and y_{min} are the maximum and minimum values of the measured data in field work, respectively.

Fig. 7 showed the R^2, RMSE and nRMSE between the measured and estimated LAI, CCC and LCC. It could be seen clearly that the estimation accuracy using the enhanced image (LAI with R^2=0.54, RMSE=0.44 and nRMSE=0.128; CCC with R^2=0.65, RMSE=0.28 and nRMSE=0.112; LCC with R^2=0.46, RMSE=3.95 and nRMSE=0.119, respectively) were higher than that using the original image (LAI with R^2=0.49, RMSE=0.47 and nRMSE=0.137; CCC with R^2=0.54, RMSE=0.32 and nRMSE=0.127; LCC with R^2=0.32, RMSE=4.19 and nRMSE=0.127, respectively). Within these three estimated results, the estimation accuracy of CCC is the highest, followed by LAI and LCC.

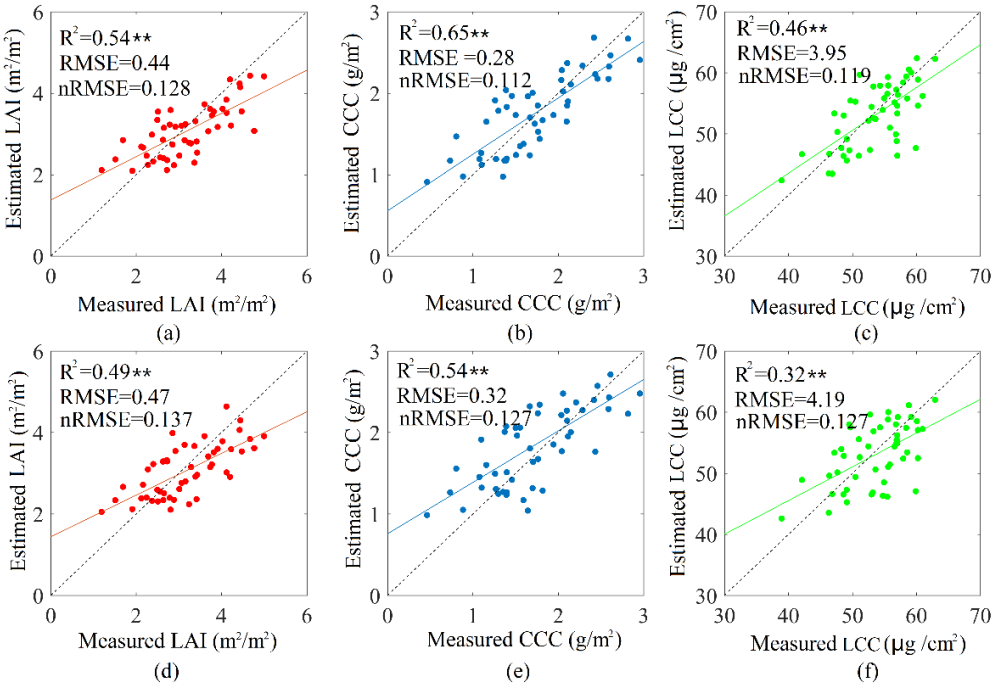

Fig. 7. Accuracy assessment results of LAI, CCC, and LCC estimated using vegetation indexes of enhanced images (a~c) and original images (d~f).

Notes: ** Correlation is significant at the 0.01 level (n=50): (a) MTCI, (b) NDI with Band 8a and Band 3, (d) RI with Band8 and Band3, (e) NDI with Band 8 and Band 3.

3.3. Retrieval results of LAI and chlorophyll content using PROSAIL model

For the reason that the remotely sensed vegetation indices such as NDVI, computed using the red and near infrared bands re of limited value since they saturate in dense vegetation (Mutanga & Skidmore, 2004), the PROSAIL radiative transfer model were used to retrieve corn canopy LAI and leaf chlorophyll content in this study. Fig. 8 was the comparation of retrieved LAI and LCC using 1023 kinds of cost functions of PROSAIL model, and there were 50 same in-situ measured samplings were used to do accuracy assessment, too. And Fig. 8 showed the R^2 distribution of retrieved LAI and LCC from the cost function using different band combinations. It could be seen from these four statistical results that the cost function using different bands were quite different, and the retrieved result with the lowest accuracy had no correlation with the measured values with R^2 is 0, actually. Comparing Fig. 8a, b, c and d, we found that the correlation coefficient (R^2) between the measured and retrieved LAI and LCC using enhanced image was significantly higher than that using the original image for all band combinations. It also showed that the corn canopy LAI and leaf chlorophyll content retrieval could be improved by the enhancement of Sentinel-2 image using the SupReME super-resolution algorithm.

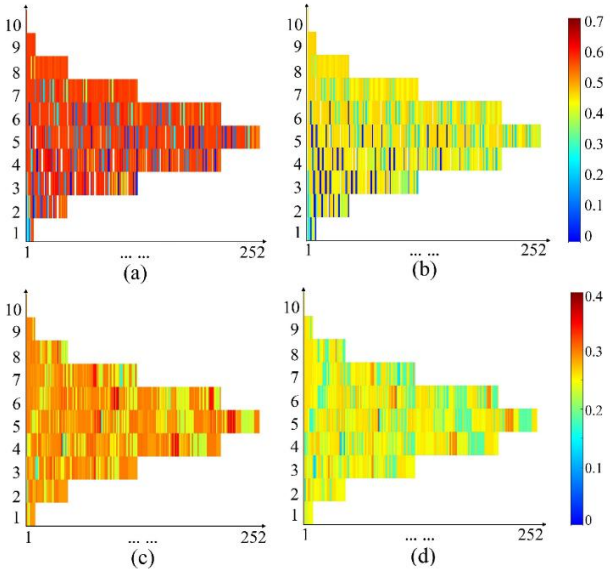

Fig. 8. The R^2 distribution results of retrieved LAI and LCC using different cost functions. The X-axis is the number of combinations of different cost functions, Y-axis is the number of bands in the cost function: (a, c) are R^2 of LAI and LCC estimated by enhanced image; (b, d) are R^2 of LAI and LCC estimated by original image.

The comparation of accuracy assessment using the best cost functions by combining different bands were as followed (Fig.9). Accuracy assessment results showed that the R^2 of measured LAI and retrieved LAI using enhanced Band 2, Band 3, Band 5 and Band 6 was 0.65, RMSE was 0.31 and nRMSE was 0.09. The R^2 of measured LAI and retrieved LAI using original Band 2, Band 4, Band 6, Band 11 and Band 12 was 0.53, RMSE was 0.49 and nRMSE was 0.143. And the R^2 of measured LCC and retrieved LCC using enhanced Band 2, Band 4, Band 6, Band 11 and Band 12 was 0.36, RMSE was 3.32 and nRMSE was 0.1. When original Band2, Band4, Band6, Band11 and Band12 were used for cost function, the R^2 of measured and retrieved LCC was 0.37, RMSE was 6.34 and nRMSE was 0.192. The CCC was calculated by the product of LAI and LCC. Accuracy assessment results showed that R^2 of measured CCC and retrieved CCC was 0.69, RMSE was 0.16 and nRMSE was 0.064 using enhanced image, while R^2 was 0.66, RMSE was 0.35 and nRMSE was 0.139 using original image. Comparatively, the retrieving accuracy using original Sentinel-2 image is lower. Although there was little difference between the R^2 of LCC retrieved from original image and enhanced image, the RMSE of LCC retrieved from original image was much higher than that of enhanced image. In generally, the corn canopy LAI and chlorophyll content retrieval accuracy using enhanced image was higher than that using original Sentinel-2 image.

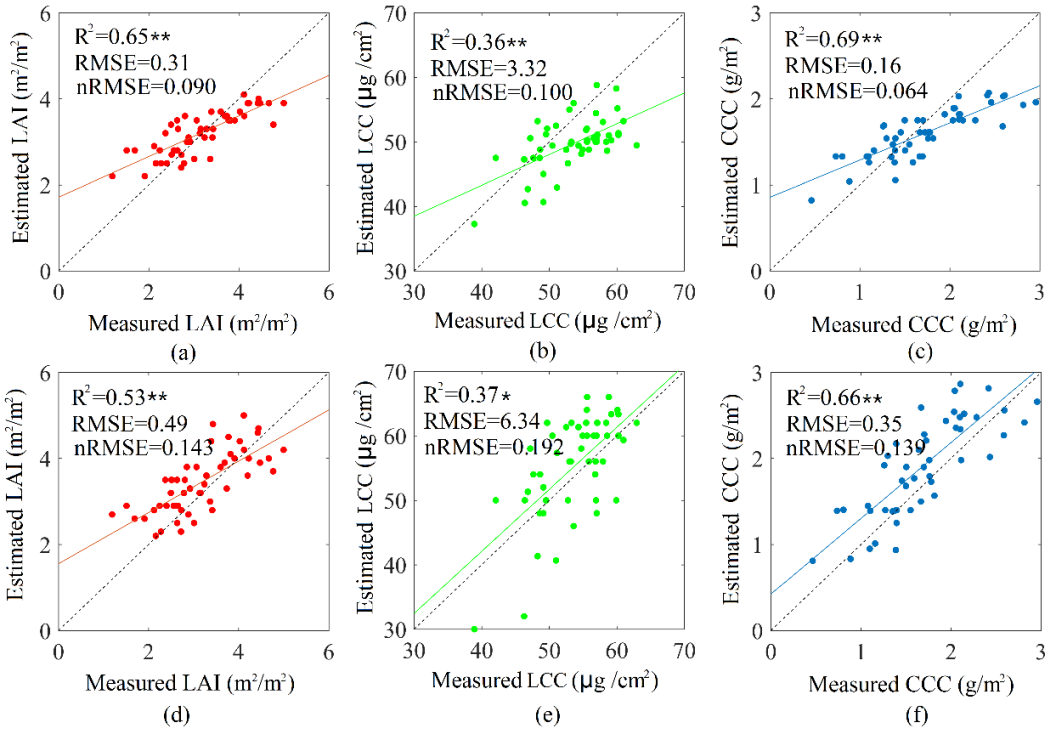

Fig. 9. Optimal results of LAI, LCC, and CCC inverted by PROSAIL-D model based on enhanced images (a~c) and original images (d~f).

Notes: ** Correlation is significant at the 0.01 level, * Correlation is significant at the 0.1 level (n=50).

4. Discussion

4.1. Comparison between enhanced image and original image

Super-resolution enhancement has been widely used in satellite image processing which could achieve the high spatial resolution images with low cost. The single-sensor imaging has the advantages of uniform imaging time and imaging angle compared with multi-sensor imaging method. In addition, single-sensor imaging would reduce the uncertainties in the fusion process and improves the efficiency and accuracy of fusion (Wang et al., 2016; Lanaras et al., 2017). Our results showed that the SupReME algorithm can be used to enhance the spatial resolution of remote sensing image, in the meantime of maintaining the spatial details and spectral variation of original image (Fig. 5).

In the comparison of super-resolution enhanced images (10m) and original low spatial resolution images (20m), we found that the R^2 of the two kind images were higher than 0.87 of six bands, and the EA were higher than 79%. Note that the EA of vegetation pixels with reflectivity less than 0.6 were higher than 97% (Table 3). On the one hand, the results showed that the reflectivity of the enhanced image kept high consistency with the original image, and the spatial details were finer. On the other hand, the accuracy of the algorithm on vegetation pixels was higher than that on non-vegetation pixels. Results showed that the pixels with poor EA were generally existed in cities, especially those buildings with glass curtain walls or other high-reflective materials (such as shopping malls, high-speed railway stations or airports). This kind of ground object had undergone mirror reflection, which made the reflectivity of the original image abnormal (more than 100%), so the reflectivity accuracy of the enhanced image was low. However, the pixels with abnormal reflectance only accounted for about 1% of all pixels, and our research target was vegetation, and consequently, the error was negligible.

The comparation of retrieved summer corn canopy LAI, CCC and LCC using enhanced image and original image was done to validate the improvement of enhanced image to the original image. The results showed that the accuracy of LAI, CCC and LCC retrieving using enhanced image were

higher than using original image (Fig. 7 and Fig. 9), especially for multi-band combination vegetation indices including at least one red-edge band with an original spatial resolution of 20m. When calculated vegetation index (MCARI, MTCI and AIVI), the enhanced image used the same band as the original image with different spatial resolution. The results (Table 4) showed that the parameter accuracy of the image enhanced by the SupReME algorithm was higher than that of the original image. Our work confirmed that the SupReME algorithm not only enhanced the spatial details of red-edge bands of Sentinel-2 image, but also improved the retrieving accuracy of summer corn canopy LAI, CCC and LCC.

4.2. Effects of combination of different bands for LAI and chlorophyll content estimation

Different vegetation canopy parameters are sensitive to different spectral wavelength. For example, the leaf chlorophyll content is sensitive to the wavelength ranging from 400nm to 800nm. LAI is more sensitive in the whole band (especially in the NIR band) and the equivalent water thickness is sensitive within the wavelength ranging from 1000nm to 2500nm (Verrelst et al., 2016). Some band combinations can increase the difference between vegetation and non-vegetation, or the vegetations with different growing condition, however some band combinations work hardly for depicting the vegetation difference (Zhao et al., 2007; Meroni et al., 2004). Therefore, the retrieval results of vegetation parameters could be different using different band combinations.

There were two kinds of band combinations were used in cost function for vegetation parameters retrieval in this study: one was the vegetation index, the other was the original bands. The red-edge bands of Sentinel-2 were incorporated especially into vegetation indexes for LAI and CCC retrieval. For the combination of two bands, Fig. 6 showed that the retrieving accuracy of LAI and CCC are high using combination using one band from Band3 to Band6 with the other band from Band6 to Band11 (excepting Band6 & Band6 combination and Band6 & Band11 combination). Moreover, we found that the combination between Band8a and Band3 of enhanced image and the combination Band8 and Band3 of original image were the optimal results. It could be seen from the Table 1 that the central wavelength of Band8 was similar to that of Band8a, but the band width was much wider. This indicated that Band8a was better than Band8 for retrieving LAI and CCC. We also calculated other popular vegetation indices which contained at least three bands and one red edge band. The results (Table 4) showed that the LAI and CCC retrieved accuracy is high using red-edge bands. It further proved the advantages and potential of multi-channel satellite images, especially those with red edge channels, such as Sentinel-2, in the application of quantitative remote sensing of vegetation.

4.3. Vegetation indexes vs. PROSAIL model

Linear models and physical models are used commonly to retrieve vegetation canopy parameters. The vegetation indexes and the PROSAIL model were used to retrieve summer corn canopy LAI, CCC and LCC in this study. The retrieval accuracy showed that both of these two methods have their own advantages for retrieving LAI, CCC and LCC. Especially, the accuracy of retrieval of summer corn canopy LAI and CCC using PROSAIL model was higher than that using vegetation indexes, and the retrieving accuracy of LCC which was on blade scale using PROSAIL model was lower than that of using vegetation indexes. As a note, there should be more in-situ measured data for developing the relationship between vegetation index and vegetation growth parameters (LAI, CCC and LCC) in the linear models. By contrast, the PROSAIL-D model based on LUT could also retrieve vegetation growth parameters without relying on ground measurements, and the accuracy had been improved.

In addition, we found that the retrieval accuracy of CCC, LAI and LCC using whether vegetation indexes or PROSAIL model were all in line of CCC > LAI > LCC (comprehensive R^2, RMSE and nRMSE). This is consistent with previous research results (Zhang et al., 2005; Darvishzadeh et al., 2008; Combal et al., 2003). LAI and CCC are canopy scaled canopy parameters, which have little difference in the uniform growth pattern, and the scale effects in pixels are not obvious. Therefore, the retrieved accuracy using PROSAIL model was better that that using

vegetation indexes. Generally, high resolution image (centimeter or millimeter level) or hyperspectral image can be inverted to obtain higher accuracy, but it is not suitable for estimating LCC of crops in large area. The linear model is only a simple regression relationship, which can obtain better results in small areas, but it cannot ignore the spatial heterogeneity of crops, so it is not suitable for estimating vegetation parameters in large areas. The PROSAIL model can be used to estimate the chlorophyll content of vegetation leaves on a large scale. However, the resolution (meter level) of satellite image differs greatly from the scale of leaf, which results in the heterogeneity of reflectance of various objects in a single pixel. Additionally, the measured data can only take the average value of a finite number of points in a single pixel. Therefore, it is more difficult to retrieve LCC at regional scale based on the physical model than LAI or CCC. There are many input parameters in the physical model itself, and the superposition of uncertainties of each parameter will also reduce the accuracy of parameter estimation. In future research, the relationship between chlorophyll content at leaf scale and mixed reflectance of pixels should be explored, and the uncertainty analysis of the PROSAIL model should be added to the process of parameter inversion to improve the accuracy of chlorophyll content inversion by the PROSAIL model, so as to extend to large regional scale.

4.4. Broader implications for agriculture applications at regional level

Finally, our results showed that the Sentinel-2 images processed by the SupReME algorithm had advantages in crop parameter inversion, especially when incorporating the red-edge band. Currently, Sentinel-2 is the only satellite available free of charge which include multiple red-edge bands with medium spatial resolution (20m). However, it is possible to improve the resolution of the red-edge band because of other 10m spatial resolution images. The SupReME algorithm produced a series of image products with a spatial resolution of 10m without increasing any cost. Because these images come from the same sensor, the uncertainty of these super-resolution enhanced images is less affected by the observation angle, imaging time and spectral response function and other reasons. It can increase spatial resolution while maintaining spectral consistency (Table 3), and the product accuracy is higher (Lanaras et al. 2017).

Due to the management style of household in China's rural areas, the area of most planting field is small. In addition, the difference of time, variety and management of crops planted by farmers, the difference between adjacent fields will be more obvious. In the application of agricultural quantitative remote sensing, the smallest unit of study is the pixel, which is used as the benchmark for the field measurement and all models. The purity or variability of the pixels has an important influence on the final results, especially when the field is fragmented (Huang et al., 2019). The spatial heterogeneity of vegetation in one pixel of 20m spatial resolution is greater than that of 10m spatial resolution (Zheng et al., 2017). Therefore, the 10m spatial resolution image could reduce the uncertainty caused by these reasons, which could be used to improve the accuracy of the crop canopy parameters retrieval, crop growth monitoring and estimation of crop yield.

Using the SupReME algorithm, we can extend it to satellite images with multi-spectral bands and different spatial resolutions, such as MODIS image and Landsat 8 image. The combination of medium resolution multi-source satellites may provide the possibility to capture the dynamic changes of crop growth at field scale which has been proved in previous studies (Huang et al., 2019, 2015) that it can effectively improve the accuracy of crop yield estimation. At the same time, the uniform high-resolution image can be obtained without increasing the cost of input, and other meteorological parameters with high spatial resolution can be retrieved, such as temperature and evapotranspiration, thus increasing the potential of practical applications and accuracy.

5. Conclusions

Sentinel-2 satellite is one of the important data sources for quantitative remote sensing of vegetation, for the reason that Sentinel-2 images are with high temporal resolution, high spatial resolution and multi-spectral bands. Since there are three different spatial resolutions for the 13 bands of Sentinel-2 image, this study is focusing on fusing different bands of Sentinel-2 images and

generated a unified high spatial resolution image. In this paper, it substantiated the reliability of SupReME algorithm in super-resolution fusing Sentinel-2 images and the fact that enhanced images could improve the accuracy of vegetation growth parameter estimation.

We enhanced the Sentinel-2 images using the SupReME algorithm for generating 10m multi-spectral images, retrieving LAI, CCC and LCC of corn canopy using linear model and physical model on large-scale regions. We draw the following conclusions: (1) The SupReME algorithm had high accuracy in fusing Sentinel-2 image, and its spectrum remained basically consistency as the original image; (2) vegetation index and cost function formed by band combination of enhanced images could achieve a higher accuracy of parameter inversion than those of original images; (3) the accuracy of LAI and CCC inversion of the physical model were higher than that of the linear model, while the accuracy of LCC inversion was lower than that of the linear model; and (4) the order of inversion accuracy of the three parameters was CCC > LAI > LCC.

We demonstrated that the enhanced image had high application value by quantitatively analyzing the results. These results indicated that SupReME algorithm was an effective and promising approach to enhance the potential and value of Sentinel-2 image at a regional scale in the North China Plains. In future research, we will apply the SupReME algorithm to the Sentinel-2 images with long time series and also consider the uncertainty of the physical model, and deep learning will be explored instead of cost function for monitoring vegetation growth and estimation of crop yield at regional scale.

Acknowledgment

This study was partly funded by the National Natural Science Foundation of China under the project 'Growth process monitoring of corn by combining time series spectral remote sensing images and terrestrial laser scanning data' (41671433), 'Estimating the leaf area index of corn in whole growth period using terrestrial LiDAR data' (41371327) and Science and Technology Facilities Council of UK- Newton Agritech Programme (Project No. ST/N006798/1). The authors would like to thank Charis Lanaras for providing SupReME code and the farmers for allowing us to make use of their fields for measurements. We also thank the journal's editors and anonymous reviewers for their efforts to improve the quality of this paper.

References

1. Afonso, M. V., Bioucas-Dias, J. M. and Figueiredo, M. A. T., 2010. Fast Image Recovery Using Variable Splitting and Constrained Optimization. IEEE TRANSACTIONS ON IMAGE PROCESSING, 19(9): 2345-2356
2. Allen, W. A., Gausman, H. W., Richardson, A. J. and Thomas, J. R., 1969. Interaction of Isotropic Light With A Compact Plant Leaf. Journal of the Optical Society of America, 59(10): 1376-1379.
3. Andreoli G. E. A., Hosgood B., 1994. Leaf Optical Properties EXperiment 93 (LOPEX93).
4. Atzberger, C. and Richter, K., 2012. Spatially constrained inversion of radiative transfer models for improved LAI mapping from future Sentinel-2 imagery. Remote Sensing of Environment, 120(SI): 208-218.
5. Bacour, C., Baret, F., Beal, D., Weiss, M. and Pavageau, K., 2006. Neural network estimation of LAI, fAPAR, fCover and LAIxLCC from top of canopy MERIS reflectance data: Principles and validation. Remote Sensing of Environment, 105(4): 313-325.
6. Baret, F., Hagolle, O., Geiger, B., Bicheron, P., Miras, B. and Huc, M., et al. 2007. LAI, fAPAR and fCover CYCLOPES global products derived from VEGETATION - Part 1: Principles of the algorithm. Remote Sensing of Environment, 110(3): 275-286.
7. Berger, K., Atzberger, C., Danner, M., D'Urso, G., Mauser, W., Vuolo, F., Hank, T., 2018. Evaluation of the PROSAIL Model Capabilities for Future Hyperspectral Model Environments: A Review Study. Remote Sensing, 10(851).
8. Boegh, E. Soegaard, H., Broge, N., Hasager, C., Jensen, N.O., Schelde, K., Thomsen, A., 2002. Airborne multispectral data for quantifying leaf area index, nitrogen concentration, and photosynthetic efficiency in agriculture. Remote Sensing of Environment, 81(PII S0034-4257(01)00342-X2-3): 179-193.
9. Bousquet, L., Lacherade, S., Jacquemoud, S. and Moya, I., 2005. Leaf BRDF measurements and model for specular and diffuse components differentiation. Remote Sensing of Environment, 98(2-3): 201-211.

10. Brantley, S.T., Zinnert, J.C. and Young, D.R., 2011. Application of hyperspectral vegetation indices to detect variations in high leaf area index temperate shrub thicket canopies. Remote Sensing of Environment, 115(2): 514-523.
11. Campbell, R.J., Mobley, K.N., Marini, R.P. and Pfeiffer, D.G., 1990. Growing Conditions Alter The Relationship Between Spad-501 Values And Apple Leaf Chlorophyll. Hortscience, 25(3): 330-331.
12. Carlson, T.N. and Ripley, D.A., 1997. On the relation between NDVI, fractional vegetation cover, and leaf area index. Remote Sensing of Environment, 62(3): 241-252.
13. Casa, R. and Jones, H.G., 2004. Retrieval of crop canopy properties: a comparison between model inversion from hyperspectral data and image classification. International Journal of Remote Sensing, 25(6): 1119-1130.
14. Chen, J.M. and Cihlar, J., 1996. Retrieving leaf area index of boreal conifer forests using landsat TM images. Remote Sensing of Environment, 55(2): 153-162.
15. Clevers, J.G.P.W. and Gitelson, A.A., 2013. Remote estimation of crop and grass chlorophyll and nitrogen content using red-edge bands on Sentinel-2 and-3. International Journal of Applied Earth Observation and Geoinformation, 23: 344-351.
16. Combal, B. Frederic, B., Weiss, M., Trubuil, A., Macé, D., Pragnère, A., Myneni, R., Knyazikhin, Y., Wang, L., 2003. Retrieval of canopy biophysical variables from bidirectional reflectance - Using prior information to solve the ill-posed inverse problem. Remote Sensing of Environment, 84(PII S0034-4257(02)00035-41): 1-15.
17. Darvishzadeh, R., Atzberger, C., Skidmore, A. and Schlerf, M., 2011. Mapping grassland leaf area index with airborne hyperspectral imagery: A comparison study of statistical approaches and inversion of radiative transfer models. ISPRS Journal of Photogrammetry and Remote Sensing, 66(6): 894-906.
18. Darvishzadeh, R., Matkan, A.A. and Ahangar, A.D., 2012. Inversion of a Radiative Transfer Model for Estimation of Rice Canopy Chlorophyll Content Using a Look-up -Table Approach. IEEE Journal of Selected Topics in Applied Earth Observations and Remote Sensing, 5(4SI): 1222-1230.
19. Darvishzadeh, R., Skidmore, A., Atzberger, C. and van Wieren, S., 2008. Estimation of vegetation LAI from hyperspectral reflectance data: Effects of soil type and plant architecture. International Journal of Applied Earth Observation and Geoinformation, 10(3): 358-373.
20. Dash, J. and Curran, P.J., 2007. Evaluation of the MERIS terrestrial chlorophyll index (MTCI). Advances in Space Research, 39(1): 100-104.
21. Daughtry, C., Walthall, C.L., Kim, M.S., de Colstoun, E.B. and McMurtrey, J.E., 2000. Estimating corn leaf chlorophyll concentration from leaf and canopy reflectance. Remote Sensing of Environment, 74(2): 229-239.
22. Delegido, J., Verrelst, J., Alonso, L. and Moreno, J., 2011. Evaluation of Sentinel-2 Red-Edge Bands for Empirical Estimation of Green LAI and Chlorophyll Content. Sensors, 11(7): 7063-7081.
23. Féret, J.B., Gitelson, A.A., Noble, S.D. and Jacquemoud, S., 2017. PROSPECT-D: Towards modeling leaf optical properties through a complete lifecycle. Remote Sensing of Environment, 193: 204-215.
24. Féret, J., Francois, C., Asner, G., Gitelson, A., Martin, R., Bidel, L., Ustin, S., Maire, G., Jacquemoud, S., 2008. PROSPECT-4 and 5: Advances in the leaf optical properties model separating photosynthetic pigments. Remote Sensing of Environment, 112(6): 3030-3043.
25. Gascon, F., Martimort, P. and Spoto, F., 2009. Sentinel-2 Optical High Resolution Mission for GMES Operational Services. Proceedings of SPIE - The International Society for Optical Engineering, 120(1):979.
26. Gastelluetchegorry, J.P., Pinel, V., Zagolski, F. and Demarez, V., 1995. Modeling radiative transfer in heterogeneous 3D vegetation canopies. Remote Sensing of Environment, 58(58):131-156.
27. Guan, K. Wu, J., Kimball, J., Anderson, M., Frolking, S., Li, B., Hain, C., B. Lobell, D., 2017. The shared and unique values of optical, fluorescence, thermal and microwave satellite data for estimating large-scale crop yields. Remote Sensing of Environment, 199: 333-349.
28. Houborg, R. and Boegh, E., 2008. Mapping leaf chlorophyll and leaf area index using inverse and forward canopy reflectance modeling and SPOT reflectance data. Remote Sensing of Environment, 112(1): 186-202.
29. Houborg, R., Soegaard, H. and Boegh, E., 2007. Combining vegetation index and model inversion methods for the extraction of key vegetation biophysical parameters using Terra and Aqua MODIS reflectance data. Remote Sensing of Environment, 106(1): 39-58.

30. Huang, J., Gómez-Danse, J.L., Huang, H., Ma, H., Wu, Q., Lewis, P.E., Liang, S., Chen, Z., Xue, J., Wu, Y., Zhao, F., Wang, J., Xie, X., 2019. Assimilation of remote sensing into crop growth models: Current status and perspectives. Agricultural and Forest Meteorology, 276-277.
31. Huang, J., Ma, H., Sedano, F., Lewis, P., Liang, S., Wu, Q. Su, W., Zhang, X. and Zhu, D., 2019. Evaluation of regional estimates of winter wheat yield by assimilating three remotely sensed reflectance datasets into the coupled WOFOST-PROSAIL model. European Journal of Agronomy, 102: 1-13.
32. Huang, J., Sedano, F., Huang, Y.B., Ma, H., Li, X., Liang, S., Tian, L., Zhang, X., Fan, J., Wu, W., 2016. Assimilating a synthetic Kalman filter leaf area index series into the WOFOST model to estimate regional winter wheat yield. Agricultural and Forest Meteorology, 216:188-202.
33. Huang, J. Ma, H., Su, W., Zhang, X., Huang, Y., Fan, J., and Wu, W., 2015. Jointly Assimilating MODIS LAI and ET Products into the SWAP Model for Winter Wheat Yield Estimation. IEEE Journal of Selected Topics in Applied Earth Observations and Remote Sensing, 8(8): 4060-4071.
34. Huang, J., Tian, L., Liang, S., Ma, H., Becker-Reshef, I., Huang, Y., Su, W., Zhang, X., Zhu, D. and Wu, W. 2015. Improving winter wheat yield estimation by assimilation of the leaf area index from Landsat TM and MODIS data into the WOFOST model. Agricultural and Forest Meteorology, 204: 106-121.
35. Jacquemoud, S., Verhoef, W., Frederic, B., Bacour, C., Zarco-Tejada, P., Asner, G., Francois, C., Ustin, S., 2009. PROSPECT plus SAIL models: A review of use for vegetation characterization. Remote Sensing of Environment, 1131(SI): S56-S66.
36. Jay, S., Maupas, F., Bendoula, R. and Gorretta, N., 2017. Retrieving LAI, chlorophyll and nitrogen contents in sugar beet crops from multi-angular optical remote sensing: Comparison of vegetation indices and PROSAIL inversion for field phenotyping. Field Crops Research, 210: 33-46.
37. Kuusk, A., 1995. A Markov-Chain Model of Canopy Reflectance. Agricultural and Forest Meteorology, 76(3-4): 221-236.
38. Lanaras, C., Bioucas-Dias, J., Baltsavias, E. and Schindler, K., 2017. Super-Resolution of Multispectral Multiresolution Images from a Single Sensor. IEEE Computer Society Conference on Computer Vision and Pattern Recognition Workshops, pp. 1505-1513.
39. Li, H., Xiao, S., Wei, F., Bin-Bin, G., Yuan-Shuai, Z., Yong-Hua, W., Chen-Yang, W., Tian-Cai, G., 2016. Improved remote sensing of leaf nitrogen concentration in winter wheat using multi-angular hyperspectral data. Remote Sensing of Environment, 174:122-133.
40. Markwell, J., Osterman, J.C. and Mitchell, J.L., 1995. Calibration of the Minolta SPAD-502 leaf chlorophyll meter. Photosynthesis Research, 46(3): 467-472.
41. Meroni, M., Colombo, R. and Panigada, C., 2004. Inversion of a radiative transfer model with hyperspectral observations for LAI mapping in poplar plantations. Remote Sensing of Environment, 92(2): 195-206.
42. Muller-Wilm, U., Louis, J., Richter, R., Gascon, F. and Niezette, M., 2013. Sentinel-2 Level 2A Prototype Processor: Architecture, Algorithms and First Results, pp. 8 pp.-8 pp.
43. Mutanga, O., & Skidmore, A. K. 2004. Narrow band vegetation indices overcome the saturation problem in biomass estimation. International journal of remote sensing, 25(19), 3999-4014.
44. Nilson, T. and Kuusk, A., 1989. A reflectance model for the homogeneous plant canopy and its inversion. Remote Sensing of Environment, 27(2): 157-167.
45. Pardo-Iguzquiza, E., Rodriguez-Galiano, V.F., Chica-Olmo, M. and Atkinson, P.M., 2011. Image fusion by spatially adaptive filtering using downscaling cokriging. ISPRS Journal of Photogrammetry and Remote Sensing, 66(3): 337-346.
46. Park, S.C., Park, M.K. and Kang, M.G., 2003. Super-resolution image reconstruction: A technical overview. IEEE Signal Processing Magazine, 20(3): 21-36.
47. Pu, R.L., Gong, P., Biging, G.S. and Larrieu, M.R., 2003. Extraction of red edge optical parameters from Hyperion data for estimation of forest leaf area index. IEEE Transactions on Geoscience and Remote Sensing, 41(42): 916-921.
48. Roy, D.P., Li, J., Zhang, H.K., Yan, L., Huang, H., and Li, Z., 2017. Examination of Sentinel 2A multi-spectral instrument (MSI) reflectance anisotropy and the suitability of a general method to normalize MSI reflectance to nadir BRDF adjusted reflectance. Remote Sensing of Environment, 199: 25-38.
49. Sibanda, M., Mutanga, O. and Rouget, M., 2015. Examining the potential of Sentinel-2 MSI spectral resolution in quantifying above ground biomass across different fertilizer treatments. ISPRS Journal of Photogrammetry and Remote Sensing, 110: 55-65.

50. Thomas, C., Ranchin, T., Wald, L. and Chanussot, J., 2008. Synthesis of multispectral images to high spatial resolution: A critical review of fusion methods based on remote sensing physics. IEEE TRANSACTIONS ON GEOSCIENCE AND Remote Sensing, 46(5): 1301-1312.
51. Turner, D.P., Cohen, W.B., Kennedy, R.E., Fassnacht, K.S. and Briggs, J.M., 1999. Relationships between leaf area index and Landsat TM spectral vegetation indices across three temperate zone sites. Remote Sensing of Environment, 70(1): 52-68.
52. Verrelst, J., Sabater, N., Pablo Rivera, J., Munoz-Mari, J., Vicent, J., Camps-Valls, G., & Moreno, J, 2016. Emulation of Leaf, Canopy and Atmosphere Radiative Transfer Models for Fast Global Sensitivity Analysis. Remote Sensing, 8(6738).
53. Vina, A., Gitelson, A.A., Nguy-Robertson, A.L. and Peng, Y., 2011. Comparison of different vegetation indices for the remote assessment of green leaf area index of crops. Remote Sensing of Environment, 115(12): 3468-3478.
54. Vivone, G., Alparone, L., Chanussot, J., Dalla Mura, M., Garzelli, A., Licciardi, G.A., Restaino, R., and Wald, L., 2015. A Critical Comparison among Pansharpening Algorithms. IEEE Transactions on Geoscience and Remote Sensing, 53(5): 2565-2586.
55. Wang, Q., Blackburn, G.A., Onojeghuo, A.O., Dash, J., Zhou, L., Zhang, Y., & Atkinson, P.M., 2017. Fusion of Landsat 8 OLI and Sentinel-2 MSI Data. IEEE Transactions on Geoscience and Remote Sensing, 55(7): 3885-3899.
56. Wang, Q., Shi, W., Atkinson, P.M. and Zhao, Y., 2015. Downscaling MODIS images with area-to-point regression kriging. Remote Sensing of Environment, 166: 191-204.
57. Wang, Q., Shi, W., Li, Z. and Atkinson, P.M., 2016. Fusion of Sentinel-2 images. Remote Sensing of Environment, 187: 241-252.
58. Welles, J.M. and Norman, J.M., 1991. Instrument for Indirect Measurement of Canopy Architecture. Agronomy Journal, 83(5): 818-825.
59. Zhang, Q.Y., Xiao, X.M., Braswell, B., Linder, E., Baret, F., and Moore, B, 2005. Estimating light absorption by chlorophyll, leaf and canopy in a deciduous broadleaf forest using MODIS data and a radiative transfer model. Remote Sensing of Environment, 99(3): 357-371.
60. Zhao, D., Huang, L., Li, J. and Qi, J., 2007. A comparative analysis of broadband and narrowband derived vegetation indices in predicting LAI and CCD of a cotton canopy. ISPRS Journal of Photogrammetry and Remote Sensing, 62(1): 25-33.
61. Zheng, H., Du, P., Chen, J., Xia, J., Li, E., Xu, Z., Li, X., and Yokoya, N., 2017. Performance Evaluation of Downscaling Sentinel-2 Imagery for Land Use and Land Cover Classification by Spectral-Spatial Features. Remote Sensing, 9(127412).